OPEN ACCESS

Daytime cooling efficiency and diurnal energy balance in Phoenix, Arizona, USA

Ariane Middel[1],*, Anthony J. Brazel[2], Shai Kaplan[2], Soe W. Myint[2]

[1]**Decision Center for a Desert City, Arizona State University, Tempe, Arizona 85287-8209, USA**
[2]**School of Geographical Sciences and Urban Planning, Arizona State University, Tempe, Arizona 85287-5302, USA**

ABSTRACT: Summer daytime cooling efficiency of various land cover is investigated for the urban core of Phoenix, Arizona, using the Local-Scale Urban Meteorological Parameterization Scheme (LUMPS). We examined the urban energy balance for 2 summer days in 2005 to analyze the daytime cooling-water use tradeoff and the timing of sensible heat reversal at night. The plausibility of the LUMPS model results was tested using remotely sensed surface temperatures from Advanced Spaceborne Thermal Emission and Reflection Radiometer (ASTER) imagery and reference evapotranspiration values from a meteorological station. Cooling efficiency was derived from sensible and latent heat flux differences. The time when the sensible heat flux turns negative (sensible heat flux transition) was calculated from LUMPS simulated hourly fluxes. Results indicate that the time when the sensible heat flux changes direction at night is strongly influenced by the heat storage capacity of different land cover types and by the amount of vegetation. Higher heat storage delayed the transition up to 3 h in the study area, while vegetation expedited the sensible heat reversal by 2 h. Cooling efficiency index results suggest that overall, the Phoenix urban core is slightly more efficient at cooling than the desert, but efficiencies do not increase much with wet fractions higher than 20%. Industrial sites with high impervious surface cover and low wet fraction have negative cooling efficiencies. Findings indicate that drier neighborhoods with heterogeneous land uses are the most efficient landscapes in balancing cooling and water use in Phoenix. However, further factors such as energy use and human vulnerability to extreme heat have to be considered in the cooling-water use tradeoff, especially under the uncertainties of future climate change.

KEY WORDS: Urban climate · Sensible heat flux transition · Cooling efficiency · LUMPS · Remote sensing · Land cover · Urban heat island · Phoenix

1. INTRODUCTION

The urban heat island (UHI) effect is probably the most intensively studied anthropogenic local change in climate (Arnfield 2003). Heat islands form when natural landscapes are urbanized. Impervious materials store a large amount of heat during the day and release it slowly at night, increasing the disparity between rural and urban temperatures, especially at night. The UHI effect has significant implications for urban residents, particularly in arid regions. Amplified local temperatures increase energy demand for air conditioning in the summer, contribute to air pollution, reduce human comfort, and increase vulnerability to extreme heat events (Harlan et al. 2006, Sarrat et al. 2006, Grimmond 2007, Hart & Sailor 2009). Mitigating the UHI effect is vital to enhance the adaptive capacity of cities in arid regions and will become increasingly important in the future with continued urban expansion and population growth under global climate uncertainty.

A substantial body of literature has focused on UHI mitigation strategies over the past decade and using urban design as an effective measure has been pro-

posed by various studies (Baker et al. 2002, Stone & Norman 2006, Coutts et al. 2007, Middel et al. 2011). An important design strategy to improve local climate in places with dry hot summers is cooling through vegetation, because evapotranspiration (*ET*) is an important cooling agent in arid environments (Bonan 2000). Pearlmutter et al. (2009) quantified the relation between vegetative surface area and corresponding latent heat flux and found that the relationship was nearly linear. Gober et al. (in press) analyzed the effects of vegetation on nighttime cooling at the Census block group scale and found that cooling rates of air temperatures at the boundary layer height in Phoenix, Arizona, double when the amount of vegetation is increased by 10%. Buyantuyev & Wu (2010) report nighttime surface temperature differences of up to 9°C between paved surfaces and vegetation in the Phoenix metropolitan area at Advanced Spaceborne Thermal Emission and Reflection Radiometer (ASTER) image scale (90 m resolution).

Previous research has shown that land cover changes can purposefully alter the thermal environment, but adding vegetation in arid regions increases irrigation requirements and raises concerns about water scarcity and conservation. Finding a balance between temperature amelioration and water conservation in mitigating heat islands is crucial to developing more sustainable landscape practices. This tradeoff was investigated by Gober et al. (2009) for selected areas in Phoenix under different land cover scenarios. Results suggest that there is a threshold beyond which increased vegetative cover does not significantly decrease UHI effects. Shashua-Bar et al. (2009) conducted a controlled experiment to analyze the cooling efficiency of different landscape strategies in the arid Negev Highlands. They chose 2 adjacent courtyard spaces with a similar geometry and materials, but different landscaping. The authors set up 2 irrigation systems to provide each courtyard with sufficient water and investigated the cooling impact of 6 combinations of trees, grass, and shade mesh. They found a combination of shade trees over grass to be the most effective strategy.

Here, we build upon this cooling-water use tradeoff research and systematically analyze the cooling characteristics of various landscapes in Phoenix. Specifically, we address the question: How does land cover influence the daytime cooling efficiency in the Phoenix urban core and the timing of sensible heat flux reversal at night? We used the Local-Scale Urban Meteorological Parameterization Scheme (LUMPS) (Grimmond & Oke 2002, Loridan et al. 2011) to model the surface energy balance above canopy as the basis

for our analysis. We tested the plausibility of our modeling results with daytime and nighttime surface temperatures from ASTER imagery and validated latent heat fluxes using reference evapotranspiration values from a nearby meteorological weather station. To investigate the daytime tradeoff between water demand of irrigated landscapes and the amount of cooling achieved, we adopted the cooling efficiency index developed by Shashua-Bar et al. (2009, 2011). Furthermore, we calculated the sensible heat flux transition time (t_0) when the sensible heat flux changes its direction from upwards to downwards at night to investigate the variability of this timing and its relation to the magnitude of the daytime integrated heat storage. Our analysis of t_0 at night and the daytime cooling efficiency of different landscapes in Phoenix will give vital insights to water stakeholders and urban planners on how vegetation can be effectively used to mitigate UHI effects under water conservation constraints.

2. STUDY AREA

The Phoenix metropolitan area is a rapidly urbanizing region in the Sonoran Desert of the southwestern United States. It is an excellent site for investigating impacts of the UHI, because it is characterized by growth and urban development (Gammage 2003). From 2000 to 2010, the population in metropolitan Phoenix grew by 29% to 4.1 million people (US Census Bureau 2010) with a low population density of about 111 people km^{-2}, making it the 13th largest metropolitan area in the United States, covering an area of 37 744 km^2. Phoenix has an arid climate with mean maximum air temperatures over 40°C in July and average daily high air temperatures above 13°C in the winter (AZMET 2011). Land use transformations due to rapid population growth over the past 50 yr have increased average daily air temperatures in the Phoenix core by almost 3.5°C (Western Regional Climate Center 2011) and steadily decreased nighttime cooling. Brazel et al. (2000) documented average minimum air temperature differences of up to 6°C between rural and urban sites for the year 1995. More recent studies reported variations in the Phoenix UHI effect between 6 and 13°C on a rural to urban gradient (Hawkins et al. 2004, Brazel et al. 2007). Urban development and associated land cover changes in Phoenix also significantly contribute to high air temperatures in extreme heat events and thus increase human vulnerability (Grossman-Clarke et al. 2010).

This study concentrates on a square area covering approximately 51 census tracts in and around downtown Phoenix (Fig. 1). The study area is composed of diverse land use and land cover classes (for more details see Fig. 2). It includes urban and suburban neighborhoods (commercial, industrial, and residential segments with different densities, see Fig. 5a) as well as desert landscape, unmanaged soil, and undeveloped areas. Altogether, the study area is a representative cross-section of typical land cover in the city of Phoenix.

3. METHODS AND MATERIALS

We use the LUMPS version 5.3 developed by Grimmond & Oke (2002) to simulate the hourly urban surface energy balance for the study area at the inerti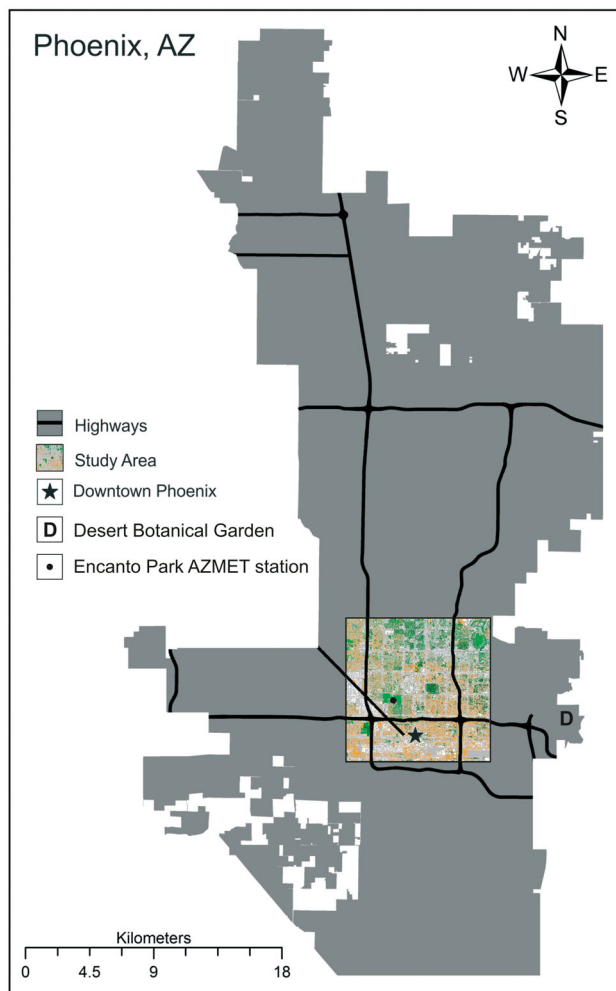al sub-layer. LUMPS models heat fluxes by partitioning the net all-wave radiation $Q^\star$ into sensible heat flux Q_H, latent heat flux Q_E, and heat storage ΔQ_S:

$$Q^\star = Q_E + Q_H + \Delta Q_S \qquad (1)$$

The model runs at a local or neighborhood scale (0.01 to 100 km^2) with few input requirements, i.e. basic land cover information (buildings, impervious surfaces, soil, grass, trees and shrubs, water) and standard weather observations (air temperature, relative humidity, incoming solar radiation, precipitation, air pressure) at flux tower height (30 m). To calculate the energy budget partitioning, LUMPS incorporates the Objective Hysteresis Model (Grimmond et al. 1991) for heat storage parameterization and the Net All-wave Radiation Parameterization (Offerle et al. 2003) for estimation of $Q^\star$. Outputs include the hourly energy budget components of sensible and latent heat fluxes, heat storage, and net all-wave radiation for the modeling period.

LUMPS is a relatively simple model. It does not take into account advection processes and anthropogenic heat, which are both assumed to be inherent in the parameterization. Yet, LUMPS has been proven to perform well in urban areas at a local scale. The model was evaluated through extensive field observations in 8 North American cities and 2 European cities (Grimmond 1992, Grimmond & Oke 1995, 1999, 2002, Offerle et al. 2006, Loridan et al. 2011). LUMPS was further validated using airborne hyperspectral images of Shanghai (Xu et al. 2008). More recently, the model has been successfully applied in Phoenix and Portland to analyze summer atmospheric heating (Middel et al. 2011), climate variability and evapotranspiration (Middel et al. in press), and cooling under different land cover scenarios and future climate change (Gober et al. 2009, in press, House-Peters & Chang 2011).

3.1. Land cover data

LUMPS 5.3 requires input for 6 land cover classes per unit of analysis: buildings, impervious surfaces, trees and shrubs, unmanaged soil, grass, and water bodies. For this study, we derived land cover from Quickbird imagery (Fig. 2a) with 4 multi-spectral bands (blue: 0.45–0.52 μm, green: 0.52–0.60 μm, red: 0.63–0.69 μm, near infrared: 0.76–0.90 μm) and 3 PCA (Principal Component Analysis) bands. The aerial image was acquired May 29, 2007 at a spatial resolution of 2.4 m. It covers approximately 89 km^2 of the central portion of the City of Phoenix. The required land cover classes (Fig. 2b) were derived using

Fig. 1. Study area in the urban core of the city of Phoenix, Arizona (Phoenix Downtown 33° 26′ 54″ N, 112° 4′ 24″ W)
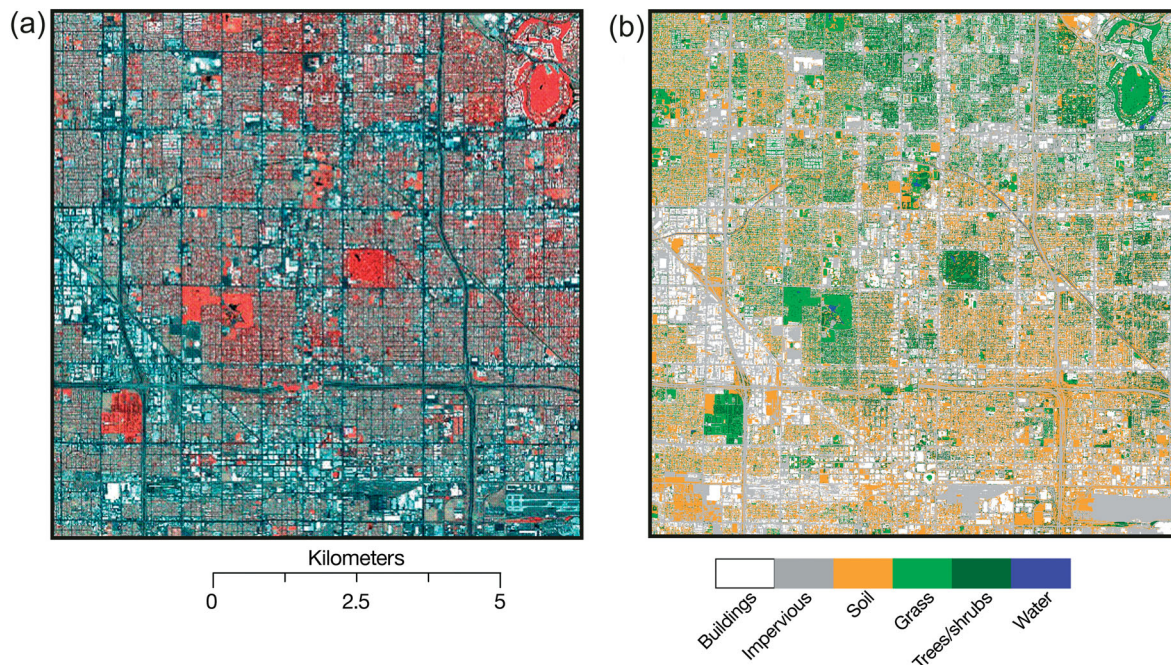
Fig. 2. Land cover classification in the study area: (a) Quickbird aerial image acquired May 29, 2007 (vegetation is displayed in red); (b) land cover classification derived from Quickbird imagery

an object-based approach developed by Myint et al. (2011) at an overall accuracy of 89.9%. The results were aggregated to areas of 90 m × 90 m resulting in a total number of 11 025 grid squares to satisfy LUMPS minimum spatial scale and to match the resolution of the ASTER image used for plausibility testing purposes. Fig. 3 summarizes the classification results for the study area. 'Impervious surfaces' is the prevailing land cover class with almost 28%. On average, buildings, soil, and grass amount to about 20% each of the total area, while trees and shrubs are less predominant, adding up to 10%. Water bodies only make up for 0.2% of the total land cover and mainly represent swimming pools in the study area.
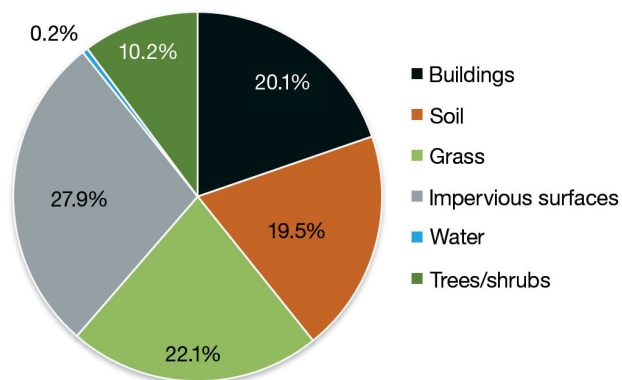

Fig. 3. Average land cover characteristics for the study area, based on a sample of 11025 squares of 90 m × 90 m

3.2. Weather data

To satisfy LUMPS weather input requirements, we obtained meteorological observations at an hourly scale from the Arizona Meteorological Network (AZMET 2011). The AZMET Encanto Park weather station is located roughly in the center of the study area and is assumed to be representative of the whole area, since detailed meteorological data were not available at a fine spatial resolution. The 1 km^2 area around the weather station has a building fraction of 11.6%, encompasses 8.6% soil, 20.3% impervious surfaces, and an overall wet fraction, i.e. grass, trees, and water bodies, of 59.5%. We chose July 6 and August 22, 2005 to test our LUMPS results, because thermal surface remote sensing data were available to us for these dates. Local weather conditions were optimal for our modeling approach: clear skies, light or no wind, no precipitation, and typical summer air temperatures for Phoenix with lows of between 23 and 27°C and afternoon highs between 40 and 42°C (Fig. 4).

3.3. Q_H transition time and cooling efficiency

We calculated t_0 (when the sensible heat flux changes its direction, in other words where $Q_H = 0$) from LUMPS hourly output. To determine the cooling
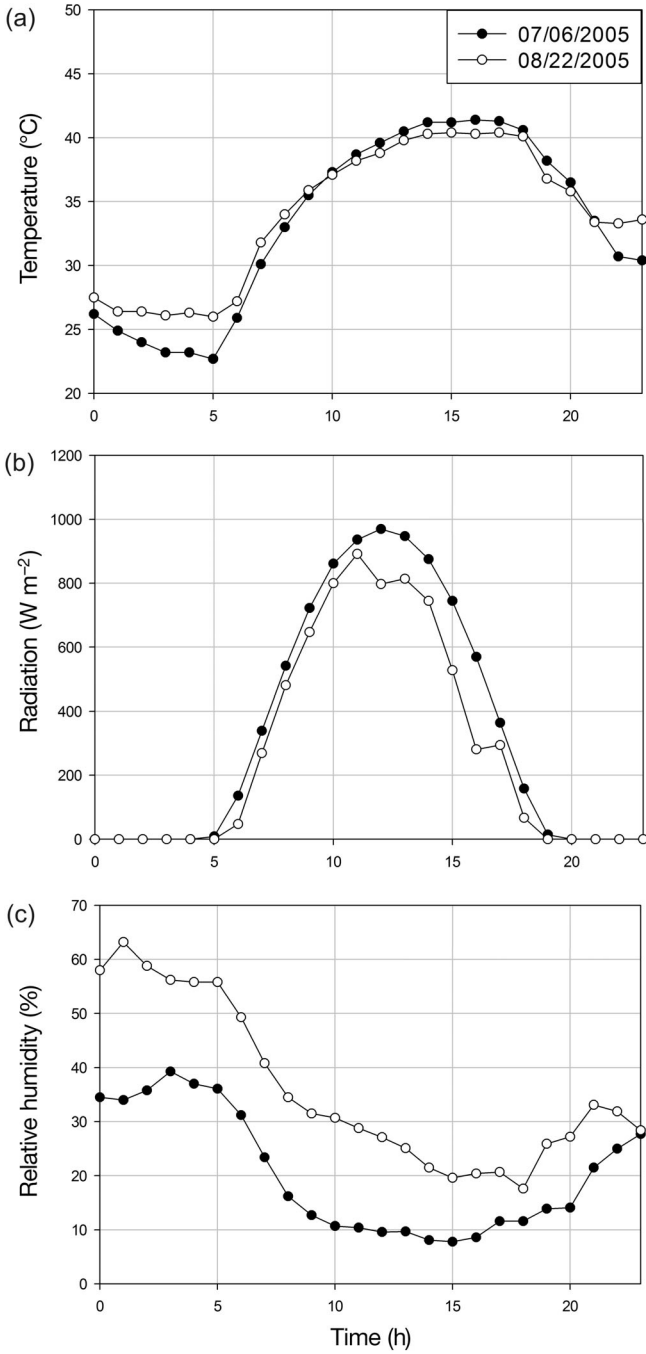
Fig. 4. Hourly meteorological observations from the AZMET (2011) Encanto Park weather station for July 6, 2005 and August 22, 2005: (a) air temperature (°C); (b) incoming solar radiation (W m^{-2}); (c) relative humidity (%)

efficiency of different landscape strategies, we adopted the evaporative cooling efficiency index f from Shashua-Bar et al. (2009, 2011). The efficiency index f describes the ratio (percent) of differences in Q_E and Q_H given in W m^{-2} between a site and a base configuration:

$$f = \frac{\Delta Q_H}{\Delta Q_E} \cdot (-100) \qquad (2)$$

We chose the desert as basic land cover, because it is the natural landscape of the study area and allows us to analyze the effects of anthropogenic changes on the urban heat and water balance. The amount of cooling per water use is calculated for each urban area from differences in average daytime Q_E, representing water use, and Q_H between each LUMPS run and a desert run.
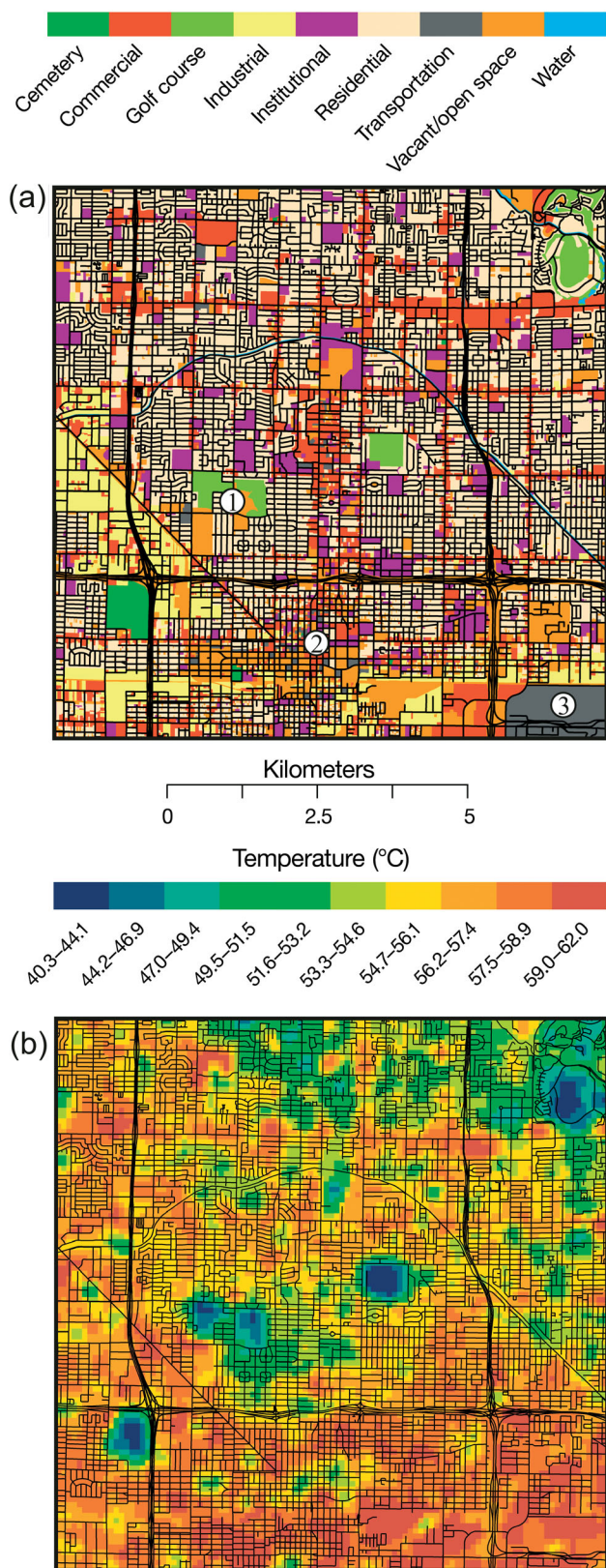
As fractions for the desert, we used 95% unmanaged soil and 5% wet fraction to estimate desert-like conditions for comparison to our urban locations. Buyantuyev & Wu (2010) indicate the natural vegetation cover of the Sonoran Desert surrounding the Phoenix area is *Larrea-Ambrosia* (a creosote/white bursage series) and a saltbush series of Sonoran Desert scrub, which experience significant interannual variability in primary productivity, spatially and temporally. Using data and results from Myint & Okin (2009), we analyzed a controlled desert scrub sample at the Desert Botanical Gardens just east of our study area (see Fig. 1) by estimating vegetation cover from Landsat imagery (30 m resolution) for June 2000, a drought year, in a preserved 0.25 km^2 area. Our sample estimate yielded 6% vegetative cover. Thus, the findings shown here probably underestimate Q_E and overestimate Q_H slightly for the desert for 2005.

4. MODEL TESTING

4.1. Sensible heat flux

Surface remote sensing has been widely used in the past to validate flux models and assess UHI effects (Weng 2009). Thermal infrared remote sensing sensors employed to retrieve land surface temperatures include Landsat TM/EMT+ (Chen et al. 2006), MODIS (Imhoff et al. 2010) to OMIS (Xu et al. 2008) and ASTER (Nichol et al. 2009, Cao et al. 2010, Cai et al. 2011). We chose ASTER imagery for our plausibility analysis, because ASTER provides more bands in the long wave and short wave infrared than other thermal sensors while still providing high spatial resolution in the visible bands. Altogether, ASTER images contain bands in the electromagnetic spectrum with a spatial resolution between 15 and 90 m.

We obtained ASTER images for the Phoenix metropolitan area for July 6, 2005 (daytime, 10:00 h) and August 22, 2005 (nighttime, 22:00 h) with a spatial resolution of 90 m. The weather conditions for these

Fig. 5. (a) Land use in the study area and ASTER images (resolution = 90 m) for (b) July 6, 2005, 10:20 h and (c) August 22, 2005, 22:20 h. ① AZMET weather station; ② downtown Phoenix; ③ Phoenix Sky Harbor International Airport

acquired dates were typical for summer days in Phoenix with no rainfall and mostly cloud-free conditions. We calculated per-pixel land surface temperatures (°C) from the 5 ASTER long wave infrared channels scaling measured radiances by per-pixel emissivity, which is calculated with the Normalized Emissivity Method (Gillespie et al. 1999, JPL 2001) as part of a Temperature Emissivity Separation (TES) algorithm. This algorithm works on 'land-leaving thermal infrared (TIR) radiance' ASTER data, which have already been corrected for atmospheric transmissivity and upwelling atmospheric path radiance (Palluconi et al. 1994).

Fig. 5a–c illustrates general characteristics of land use and day and night ASTER surface temperatures. Land use characteristics were mapped from Maricopa Association of Governments (MAG) 2009 land use data. Three golf courses and a large cemetery highlight the coolest areas both day and night. During daytime these locales are some 22°C cooler than commercial and downtown urban surfaces, and have the highest NDVI (Normalized Difference Vegetation Index) values. The more mesic neighborhoods in the north of the scene, around Encanto Park, and to

the northeast and east are also cooler than downtown by some 10 to 15°C. The nighttime image shows, as expected, very warm features of the downtown and mid-town area, the commercial strip to the west, airport premises to the extreme southeast corner, and areas adjacent to and along major transportation streets, such as shopping malls and commercial developments. These areas are 8 to 12°C warmer than residential, cemetery, and golf course locations, with the extreme case of the airport runway being in excess of 12°C difference.

The LUMPS Q_H was correlated with daytime and nighttime ASTER surface temperatures as shown in Fig. 6, and yielded R^2 values of 0.53. Note for the nighttime graph, a cluster of points exceeding 35°C is associated with positive Q_H values. These values are related to the high impervious surfaces areas in the image. This delay of t_0 has been reported by Grimmond & Oke (2002) and Harman & Belcher (2006). In the daytime graph, a group of points have lower Q_H, yet very high surface temperatures. We found that these data result from points centered on very large, homogeneous impervious areas (airport, transportation center, extensive shopping parking areas). It is possible that the anthropogenic heat flux (Q_F), not included in the LUMPS version we used, and the very high fraction of one land cover type (>75% impervious) could account for the outlying points in Fig. 6. Comparing Shanghai surface temperatures to LUMPS outputs and outputs from a model using the aerodynamic resistance method (ARM), Xu et al. (2008) found a similar anomaly for industrial areas whereby the anthropogenic heat flux Q_F appeared to elevate surface temperatures by 10 K and the LUMPS model yielded values 140 W m^{-2} lower than

the ARM method. Phoenix typically experiences only ca. 30 to 35 W m^{-2} for Q_F in the summer (Grossman-Clarke et al. 2005), which could account for some, but not all, of the anomaly of Q_H versus temperatures shown in Fig. 6 (which approaches 60 W m^{-2}). This highly anomalous value is understandable in the context of the extreme heat source area noted above. Another possible explanation for the unexpected deviations is that the Encanto Park AZMET weather station is located in a greener neighborhood. The station data do not reflect the atmospheric conditions over extended areas with high heat capacity and conductivity very well. Overall, Fig. 6 suggests that there is an association between sensible heating of the atmosphere and variations in surface temperatures across the urban area both day and night. The relationship, however, is not exclusive, because urban surfaces and atmospheric processes are complex, but we have no means of analyzing these with LUMPS.

4.2 Latent heat flux

The AZMET network offers procedures to water users and turf managers for calculating estimates of properly watered Bermuda grass turf based on crop coefficients K_C for warm season grass and reference evapotranspiration ET_0 derived from Penman-Monteith equations (Brown 1998). We determined a turf watered scenario from the AZMET July 6 and August 22, 2005 data for Encanto Park using $K_C =$ 0.6 (properly watered) and the standard value of ET_0 provided for both days. The AZMET value refers to a uniform grass surface. We also assumed
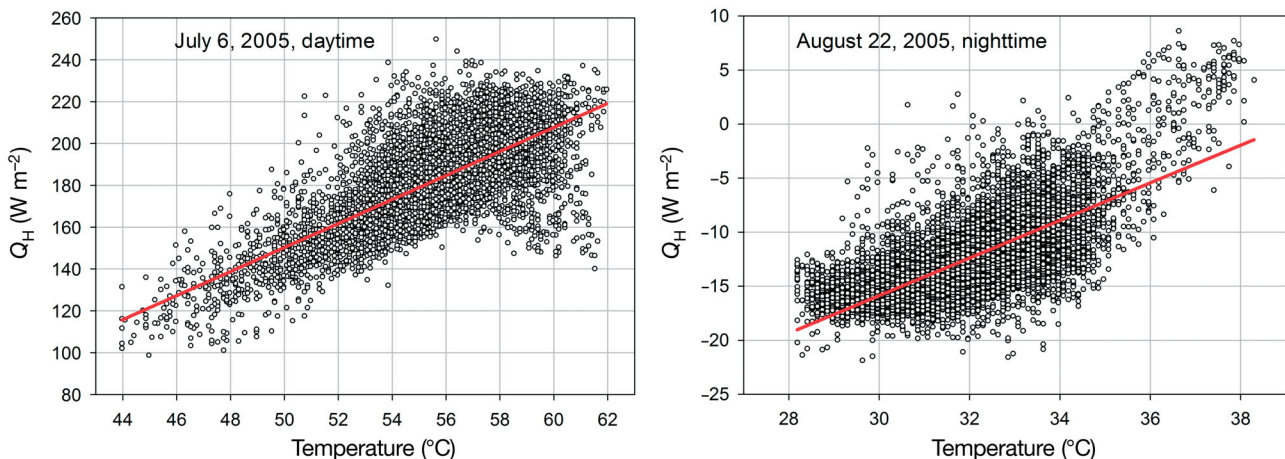

Fig. 6. Correlations between temperature and sensible heat flux (Q_H) in the study area for July 6, 2005, daytime ($R^2 = 0.53$) and August 22, 2005, nighttime ($R^2 = 0.53$). Temperatures are based on ASTER images and Q_H on LUMPS model simulation of the urban surface energy balance

the biweekly (once every 2 wk) flood irrigation schedule maintained properly watered landscapes. This yielded values for *ET* of 4.41 and 3.96 mm d^{-1} for July 6 and August 22 respectively, with lowered *ET* resulting from the cooler, more humid day of the August 22 with its lower solar radiation. We determined LUMPS Q_E estimates converted to *ET* in mm d^{-1} for a ca. 0.16 km^2 area (nine 90 m pixels) around the station. Adjusting the AZMET turf estimates by the vegetation fraction of the area under investigation (vegetation fraction ranges from 0.69 to 0.89) yields a range of 3.04 to 3.92 mm d^{-1} for July 6 and 2.73 to 3.52 mm d^{-1} for August 22. Although certainly not a definitive test of the LUMPS model, for areas of high vegetation fraction the model appears to perform well, capturing the magnitude and temporal variability, which is between 1 and 4% of the AZMET estimates.

5. RESULTS AND DISCUSSION

5.1. Sensible heat flux transition time

In July, t_0 ranges from 18:45 to 22:00 h. The sensible heat reversal in August starts later (20:00 h) and the time frame is smaller. Our simulation results suggest that t_0 is highly correlated to the daytime total heat storage between 05:00 and 19:00 h (Fig. 7). Areas with high impervious surface fraction build up more heat storage during the day, which delays the Q_H transition at night. Daytime total integrated heat storage and t_0 are highly correlated with R^2 = 0.97 in July and R^2 = 0.89 in August.

The time at which the sensible heat flux becomes negative is delayed in areas with high storage heat, but accelerated in highly vegetated areas (Fig. 8). The relationship between wet fraction and Q_H transition times t_0 is influenced by other land cover fractions (impervious, soil, and buildings) in the mix (Middel et al. in press). On average, the Q_H transition starts up to 2 h earlier in July for areas with a high wet fraction and up to 1 h earlier in August. Fig. 8 suggests that the cooling capacity of vegetation depends on atmospheric conditions and is reduced in August compared to July. August is later in the summer, incoming solar radiation is lower, and days are moister. Therefore, the wet fraction shows less influence on the timing of Q_H transition.

5.2. Energy budget

Tables 1 & 2 summarize the mean, maximum and minimum land cover fractions, flux partitioning, and daily *ET* for the entire study area (N = 11 025 pixels). For this older, central core area of the city of Phoenix, the average wet fraction is 32%, of which an average of 10% is trees and 22% is grass. We chose July 6, 2005 to analyze hourly energy fluxes and the flux ratios of Q_E, Q_H, and ΔQs to $Q^\star$ for 3 types of energy regimes in our study area in comparison to the desert scenario. These 3 sample areas, marked on Fig. 9 and listed in Table 3, group into distinct regimes in the urban environment and can be classified into local climate zones (LCZ) according to Stewart & Oke (2010). Sample area 1 (mesic, open-set, low-rise LCZ) is in a residential location with flood irrigation adja-
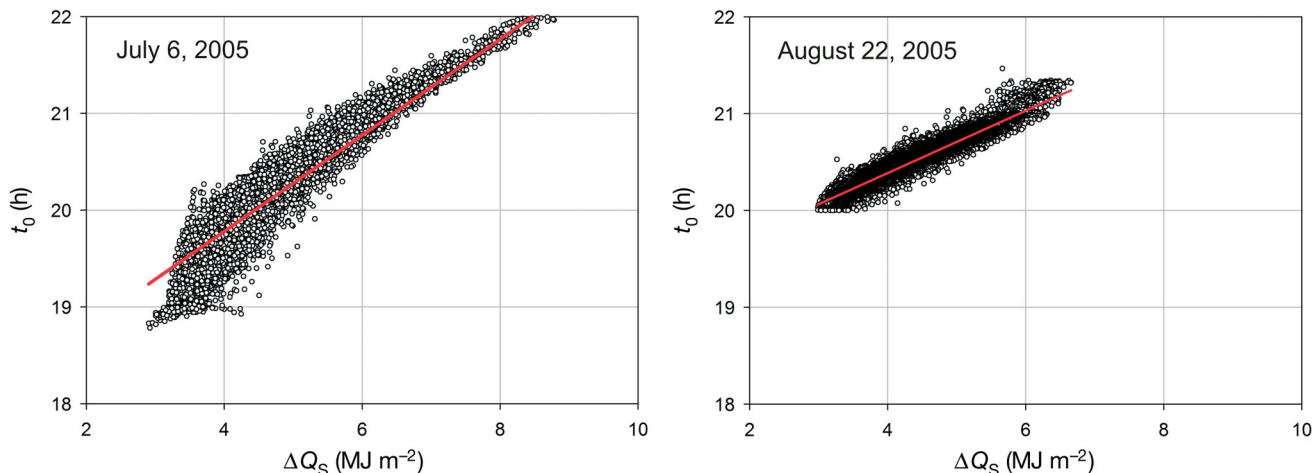

Fig. 7. Daytime total heat storage (ΔQ_S) vs. sensible heat flux transition time (t_0) in the study area for July 6, 2005 (R^2 = 0.97) and August 22, 2005 (R^2 = 0.89). Values for ΔQ_S are integrated for 05:00–19:00 h, when net all-wave radiation $Q^\star > 0$
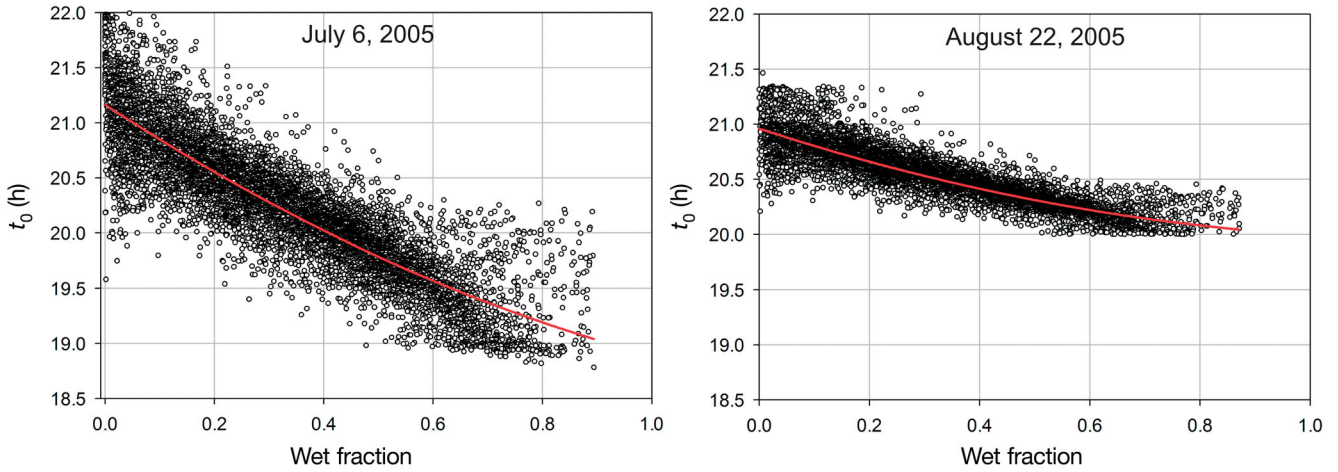
Fig. 8. Wet fraction (grass, trees, and water bodies) vs. sensible heat flux transition time (t_0) in the study area for July 6, 2005 ($R^2 = 0.78$) and August 22, 2005 ($R^2 = 0.76$)

Table 1. Land cover characteristics, evapotranspiration (ET), and heat flux partitioning for the study area, based on a sample of 11025 squares of 90 m × 90 m, for July 6, 2005. $Q^\star$: Net all-wave radiation; Q_H: sensible heat flux; Q_E: latent heat flux; ΔQ_S: heat storage

	Buildings	Soil	Grass	Impervious	Water	Trees	Daily ET (mm)	$Q_H/Q^\star$	$Q_E/Q^\star$	$Q_S/Q^\star$
Mean	0.200	0.195	0.221	0.279	0.002	0.102	1.734	0.382	0.225	0.394
Max.	0.732	0.797	0.847	0.948	0.053	0.461	3.743	0.550	0.520	0.660
Min.	0.000	0.016	0.000	0.003	0.000	0.000	0.664	0.210	0.060	0.250

Table 2. Land cover characteristics, ET, and heat flux partitioning for the study area, based on a sample of 11025 squares of 90 m × 90 m^2, for August 22, 2005. See Table 1 legend for explanation of symbols

	Buildings	Soil	Grass	Impervious	Water	Trees	Daily ET (mm)	$Q_H/Q^\star$	$Q_E/Q^\star$	$Q_S/Q^\star$
Mean	0.200	0.195	0.221	0.279	0.002	0.102	1.620	0.431	0.252	0.317
Max.	0.732	0.797	0.847	0.948	0.053	0.461	3.457	0.546	0.532	0.574
Min.	0.000	0.016	0.000	0.003	0.000	0.000	0.645	0.246	0.087	0.200

cent to a golf course. Sample area 2 (dry, open-set, low-rise LCZ) resembles many sites of urban, dry residential areas near commercial, transportation, and downtown locations, and has been the focus of concerns about heat vulnerability; greening has been suggested as a mitigative measure against the heat (Harlan et al. 2006, Chow & Brazel 2012). Sample area 3 (bare concrete LCZ) is Sky Harbor Airport. This site has of 80.9% impervious surface cover and 19.1% soil, no buildings or vegetation. In comparison, the desert site (sample area 4) can be classified as bare soil LCZ with 95% soil and only 5% trees (Table 3).

Figs. 10 & 11 show the LUMPS energy budget results for the 3 chosen landscapes, in comparison with the desert. The results for the urban landscapes are what would be expected, given the extremes of lush, flood irrigated, older residential landscapes in Phoenix with wet fractions >0.6 versus open paved urban surfaces with high impervious cover (0.81) at the airport. Compared to the airport, the mesic open-set low-rise LCZ site has almost an order of magnitude higher Q_E (Fig. 10) with a Q_E to $Q^\star$ ratio of 0.41 (Fig. 11), similar to Grimmond & Oke's (1999) Chicago and Sacramento values (C95 = 0.37 and S91 = 0.33, respectively). Moreover, the area has half the heat storage ΔQ_S, considerably less Q_H during the daytime, and slightly less $Q^\star$ (Fig. 10). The daytime ET estimates converted from Q_E range from 0.63 to 3.81 mm d^{-1}. The bare concrete LCZ site does have some soil, but a wet
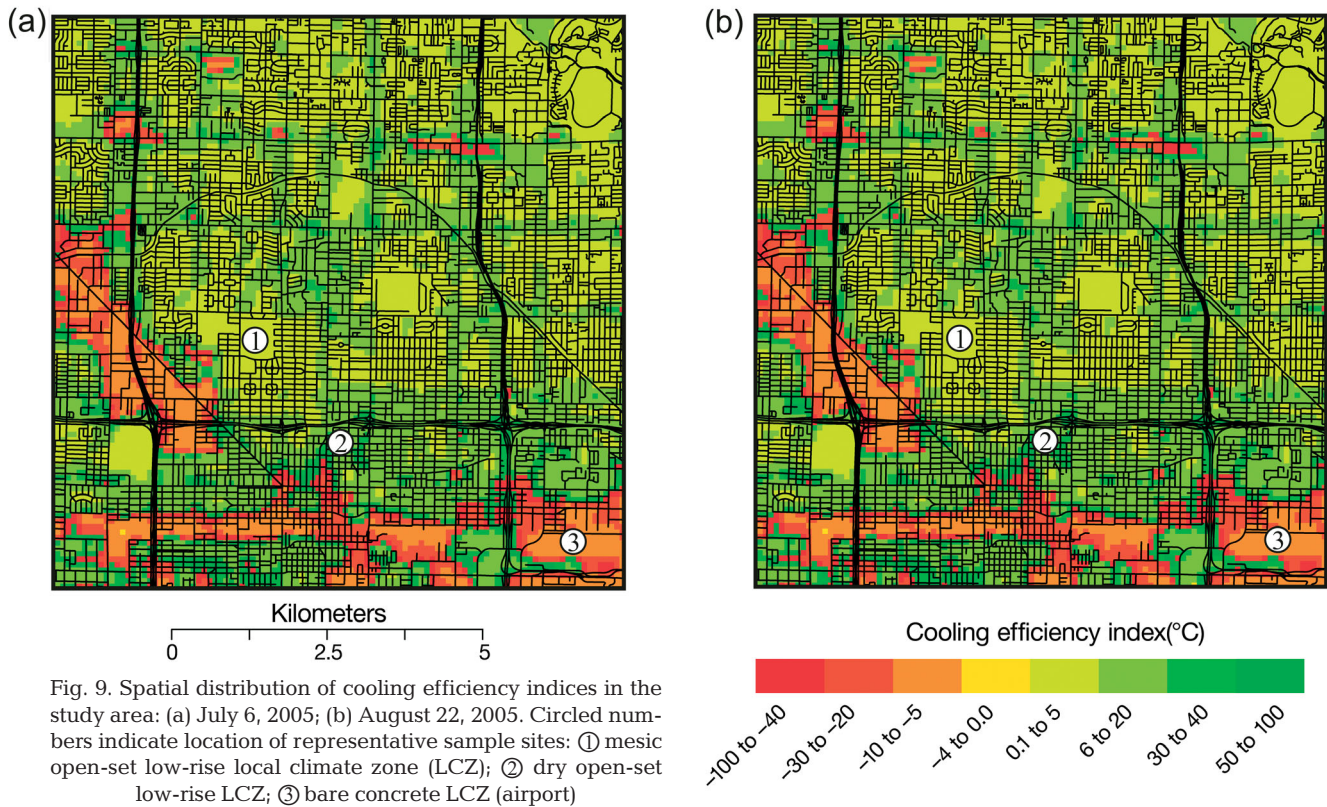
Fig. 9. Spatial distribution of cooling efficiency indices in the study area: (a) July 6, 2005; (b) August 22, 2005. Circled numbers indicate location of representative sample sites: ① mesic open-set low-rise local climate zone (LCZ); ② dry open-set low-rise LCZ; ③ bare concrete LCZ (airport)

Table 3. Characteristics of 3 sample landscapes (see Fig. 9 for location) in comparison to the desert (see Fig. 1 for location), showing land cover fractions, day and nighttime surface temperatures (°C) and calculated cooling efficiency. Sample landscape temperatures are based on ASTER images for the Phoenix metropolitan area at 10:00 h on July 6, 2005 and 22:00 h on August 22, 2005; values for desert are extrapolated

	Buildings	Impervious	Soil	Trees	Grass	Water	T_{day}	T_{night}	Cooling efficiency
Mesic (1)	0.115	0.095	0.076	0.286	0.426	0.002	45.7	30.4	3.381
Dry (2)	0.210	0.318	0.383	0.025	0.064	0.000	58.5	37.4	57.632
Bare concrete (3)	0.000	0.809	0.191	0.000	0.000	0.000	58.7	34.1	−13.049
Desert (4)	0.000	0.000	0.950	0.050	0.000	0.000	>62.0	<28.0	–

fraction of zero. The resultant Q_E to Q^* ratio of 0.07 (Fig. 11) is similar to a Grimmond & Oke's (1999) ratio for their Mexico City urban site measurements (Me93) of 0.04. The dry open-set low-rise LCZ site represents more balance between Q_H and Q_E. Q_H is lower, Q_E is slightly higher, and ΔQ_S is higher compared to corresponding fluxes of the desert (Fig. 10). Q_E of the dry site is almost 4 times lower than for the mesic site, and Q_H is correspondingly higher. From 08:00 to 22:00 h, the mainly impervious site shows continued positive Q_H, whereas the mesic and desert sites cool down and the dry area shows negative Q_H at this time. ASTER surface temperatures from Fig. 5b–c for the sample areas show that the mainly impervious area and the dry neighborhood are indeed warmer at night than

the mesic and desert sites (Table 3), but a huge reduction in daytime water use is realized. The general tradeoff for daytime is indicated by comparing values of Q_E and temperature for mesic ($Q_E = 245$ W m^{-2}; 45.7°C), impervious ($Q_E = 42$ W m^{-2}; 58.5°C), dry ($Q_E = 75$ W m^{-2}; 58.7°C), and desert ($Q_E = 73$ W m^{-2}; >62.0°C) sites.

5.3. Cooling efficiency

Using the cooling efficiency index after Shashua-Bar et al. (2009, 2011) we estimated the ratio between the sensible heat removed from the atmosphere and the amount of water supplied to it for each study
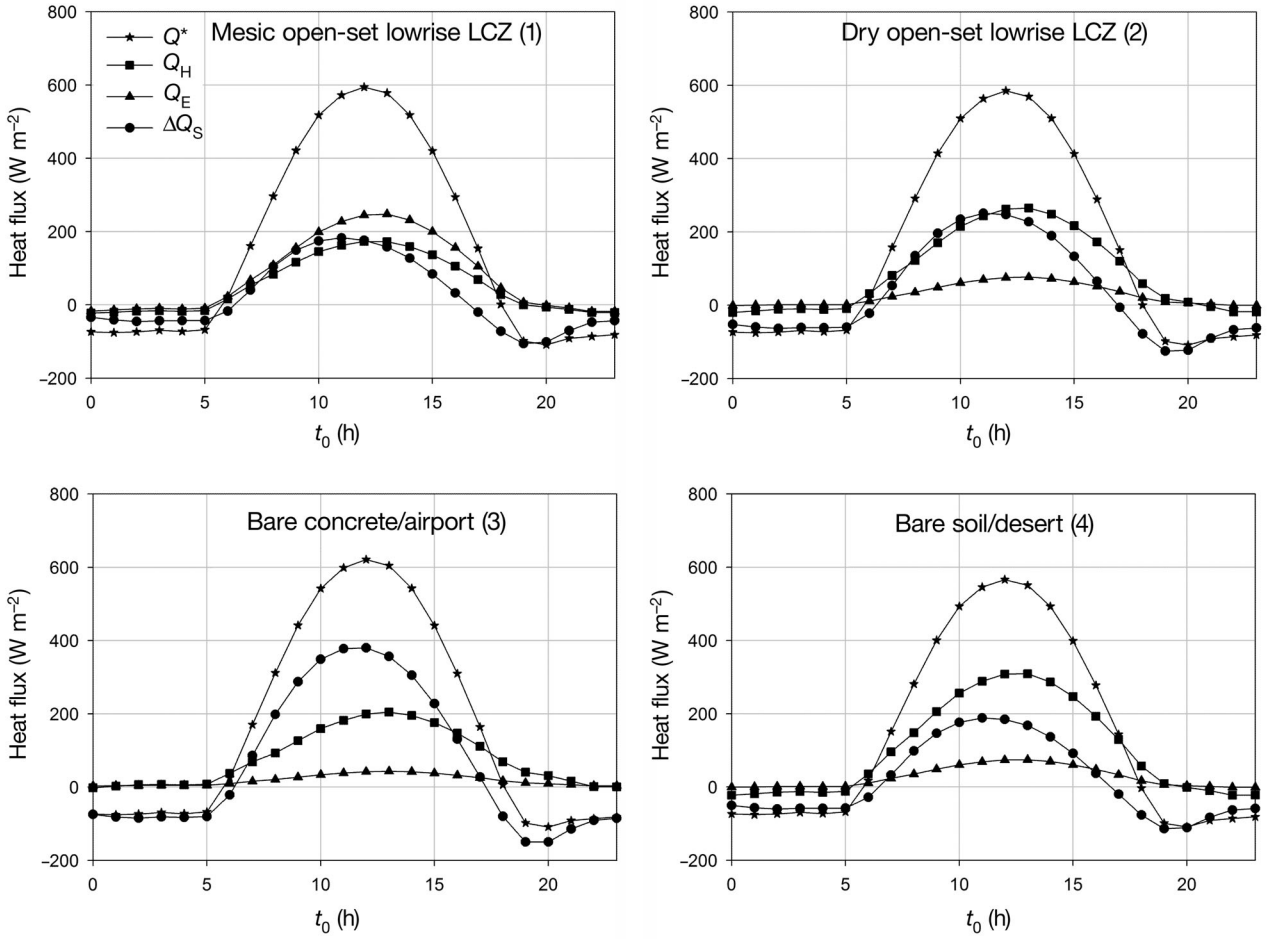
Fig. 10. Diurnal heat fluxes for 3 representative sample sites and the desert for July 6, 2005

area. Mathematically, the cooling efficiency index f is an asymptotic function. The curve increases or decreases until it approximates a certain value where it levels off and grows without bounds. In our case, the asymptote is the desert scenario. As wet fraction decreases, Q_E is reduced towards the reference desert Q_E and eventually $|\Delta Q_E| < 1$. With ΔQ_E getting infinitesimally small and $|\Delta Q_H| \geq 1$, the efficiency index

approaches $+\infty$ or $-\infty$. This singularity in the equation leads to difficulties when Q_E approaches the reference Q_E for sites that have a similar wet fraction as our desert site, because f then becomes independent of ΔQ_H. We amplify on the utility of f and use it over the entire range of possible outcomes for Phoenix, whereas Shashua-Bar et al. (2009, 2011) only investigated a certain a range.
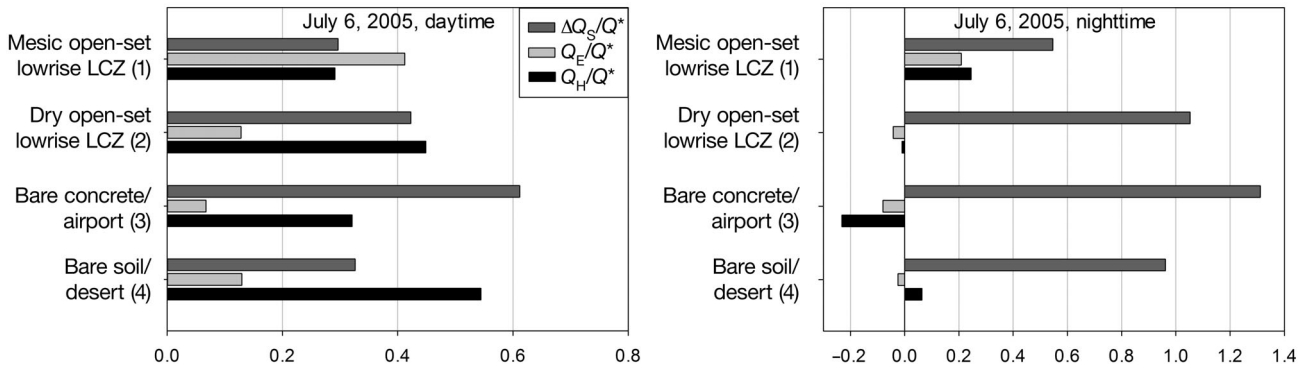

Fig. 11. Heat flux partitioning for representative sample sites in different local climate zones (LCZ) and the desert

Fig. 12 shows the efficiency index graph for our 11 025 study sites. The data separate into 2 curves: points that have a higher cooling efficiency index than the desert and points with negative efficiency compared to the desert. The cluster of points with less cooling efficiency consists of study sites with high impervious surface cover (>0.6) and low wet fraction. These sites are mainly located in the industrial zones of the study area and at the Phoenix airport, Sample site 3 (Fig. 9). Most parts of the study area have a positive efficiency index, but cooling efficiencies do not increase with wet fractions higher than 0.2 and asymptotically approach a horizontal line ($f \sim 3.0$). The graph suggests that overall, the Phoenix urban core is slightly more cooling efficient than the desert, but adding vegetation to already mesic neighborhoods does not increase efficiency. In fact, the most efficient sites at cooling with minimal water consumption are dry areas such as Sample site 2. These sites are mainly located in areas of high land use mix (compare Figs. 9 & 5a).

Findings suggest that dry neighborhoods with heterogeneous land uses are the most efficient landscapes in balancing cooling and water use. However, the efficiency index is not a measure of absolute temperatures. Although from a climatic water-temperature tradeoff aspect, dry landscaping is more efficient than high water demand mesic land cover, temperatures in drier neighborhoods are much higher and may extend beyond an unacceptable temperature comfort threshold (see Table 3). Thus, another tradeoff problem that remains to be solved from an urban design perspective is the balance between the cooling efficiency of landscapes determined here and human vulnerability effects of extreme temperatures.

6. CONCLUSIONS

The cooling efficiency index of Shashua-Bar et al. (2009, 2011) provides a concept to compare ET and atmospheric heating or cooling from the flux balance between Q_E and Q_H in the context of a tradeoff of water application to landscapes and the response of sensible heating of the atmosphere contrasted with, in our case, a natural desert setting. We realize the index was developed under a small-scale, controlled experiment, but it appears useful for these urban scale analyses as well. However, future refinement of the efficiency index should include ΔQ_S in the efficiency estimation to account for heat retention that leads to warming the atmosphere at night.

We have established the general correspondence of surface satellite-derived temperatures to outcomes of Q_H from the LUMPS model at a fine spatial resolution, resulting in statistically significant relationships. We recognize that the new Surface Urban Energy and Water Balance Scheme (SUEWS) (Järvi et al. 2011) would provide better evaluations of the Q_E flux for Phoenix. This approach remains for further study, but it is encouraging that fine resolution output of LUMPS for the well-watered case generally compares well to estimates of ET_0 from standard water user approaches that have been developed for this area. At this time, we do not have the means of testing the model over a large range of vegetative fractions in the study area, especially for the drier, more variable landscapes. To a degree, comparison of Q_H versus ASTER temperatures indirectly tests the model. A thorough test of the LUMPS models is forthcoming with the new positioning of a flux tower in a drier neighborhood of central Phoenix. We also acknowledge that we only use one
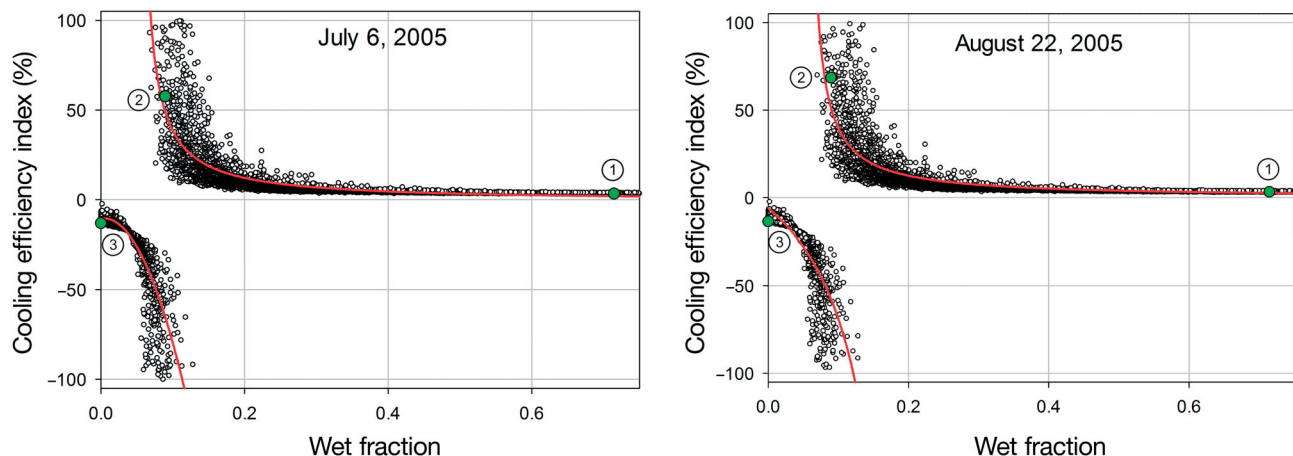

Fig. 12. Cooling efficiency index for all sites in the study area and representative sample sites: ① mesic open-set low-rise LCZ; ② dry open-set low-rise LCZ; ③ bare concrete LCZ. A rational equation curve fit yields $R^2 = 0.68$ for July 6 and $R^2 = 0.72$ for August 22

weather station that is assumed to be representative of the study area. The weather station is located near a park and thus its measurements are influenced by a greener neighborhood. By using the same input air temperatures for all sites, we neglect the feedback of the heat fluxes on atmospheric conditions. In that sense, our analysis is a sensitivity study regarding the influence of land cover variability in Phoenix on the LUMPS modeling results.

Our results indicate that the nighttime Q_H transition in the inertial sub-layer is directly related to ΔQ_S and inversely related to the wet fraction of the landscape. In addition, the relationship between cooling efficiency and wet fraction reveals imbalances of cooling relative to water transferred into the atmosphere across the study area. Drier areas have the highest cooling efficiency, i.e. the optimal tradeoff between cooling and water use, and are mainly located in areas of high land use mix. However, Ruddell et al. (2010) and Chow et al. (2012) revealed that drier landscapes in Phoenix are areas of high heat vulnerability, considering that these neighborhoods are inhabited mainly by elderly, minority, and low-income residents. When only cooling efficiency is analyzed, dry areas prove to be the most efficient; yet, when considering human vulnerability, residents of dry areas are at risk because they do not have the monetary resources needed to combat dangerous heat waves. Since the Phoenix summer is already uncomfortably hot, tracking heat intensity patterns is very important to help avoid human health risks (Harlan & Ruddell 2011). In addition to these multiple tradeoffs, there are further factors to consider, such as energy use and costs, and the effects of future climate change that may exacerbate the tradeoffs of heat vulnerability and water use, particularly with the impending drier, warmer climate predicted for the southwest USA (Karl et al. 2009). Multiple, perhaps contrasting, policies may be proposed for these scenarios and decision makers will have to determine optimal approaches for the future of the Phoenix metropolitan area, assessing the tradeoff of cooling-water use while considering vulnerability.

LITERATURE CITED

Arnfield AJ (2003) Two decades of urban climate research: a review of turbulence, exchanges of energy and water, and the urban heat island. Int J Climatol 23:1–26

AZMET (The Arizona Meteorological Network) (2011) http://ag.arizona.edu/azmet/

Baker LA, Brazel AJ, Selover N, Martin C and others (2002) Urbanization and warming of Phoenix (Arizona, USA): impacts, feedbacks and mitigation. Urban Ecosyst 6:183–203

Bonan GB (2000) The microclimates of a suburban Colorado (USA) landscape and implications for planning and design. Landsc Urban Plan 49:97–114

Brazel AJ, Selover N, Vose R, Heisler G (2000) The tale of two cities: Phoenix and Baltimore urban LTERs. Clim Res 15:123–135

Brazel AJ, Gober P, Lee SH, Grossman-Clarke S, Zehnder J, Hedquist B, Comparri E (2007) Determinants of changes in the regional urban heat island in Metropolitan Phoenix (Arizona, USA) between 1990 and 2004. Clim Res 33:171–182

Brown PW (1998) AZMET computation of reference crop evapotranspiration. ag.arizona.edu/azmet/et2.htm

Buyantuyev A, Wu J (2010) Urban heat islands and landscape heterogeneity: linking spatiotemporal variations in surface temperatures to land-cover and socioeconomic patterns. Landscape Ecol 25:17–33

Cai G, Du M, Xue Y (2011) Monitoring of urban heat island effect in Beijing combining ASTER and TM data. Int J Remote Sens 32:1213–1232

Cao X, Onishi A, Chen J, Imura H (2010) Quantifying the cool island intensity of urban parks using ASTER and IKONOS data. Landsc Urban Plan 96:224–231

Chen X, Zhao H, Li P, Yin Z (2006) Remote sensing image-based analysis of the relationship between urban heat island and land use/cover changes. Remote Sens Environ 104:133–146

Chow WTL, Brazel AJ (2012) Assessing xeriscaping as a sustainable heat island mitigation approach for a desert city. Build Environ 47:170–181

Chow WTL, Chuang WC, Gober P (2012) Vulnerability to extreme heat in metropolitan Phoenix: Spatial, temporal, and demographic dimensions. Prof Geogr 64:286–302

Coutts AM, Beringer J, Tapper NJ (2007) Impact of increasing urban density on local climate: spatial and temporal variations in the surface energy balance in Melbourne, Australia. J Appl Meteorol Climatol 46:477–493

Gammage G Jr (2003) Phoenix in perspective: reflections of developing the desert, 2nd edn. Herberger Center for Design Excellence, Arizona State University, Tempe, AZ

Gillespie AR, Rokugawa S, Hook SJ, Matsunaga T, Kahle AB (1999) Temperature/emissivity separation algorithm theoretical basis document, Version 2.4. prepared under NASA Contract NAS5-31372, NASA, Washington, DC

Gober P, Brazel A, Quay R, Myint S, Grossman-Clarke S, Miller A, Rossi S (2009) Using watered landscapes to manipulate urban heat island effects. J Am Plann Assoc 76:109–121

Gober P, Middel A, Brazel AJ, Myint SW, Chang H, Duh JD, House-Peters L (in press) Tradeoffs between water conservation and temperature amelioration in Phoenix and Portland: implications for urban sustainability. Urban Geogr

Grimmond CS (1992) The suburban energy balance: methodological considerations and results for a mid-

latitude west coast city under winter and spring conditions. Int J Climatol 12:481–497

Grimmond CSB (2007) Urbanization and global environmental change: local effects of urban warming. Geogr J 173:83–88

Grimmond CS, Oke TR (1995) Comparison of heat fluxes from summertime observations in the suburbs of four North American cities. J Appl Meteorol 34:873–889

Grimmond CSB, Oke TR (1999) Heat storage in urban areas: local-scale observations and evaluation of a simple model. J Appl Meteorol 38:922–940

Grimmond CSB, Oke TR (2002) Turbulent heat fluxes in urban areas: observations and a local-scale urban meteorological parameterization scheme (LUMPS). J Appl Meteorol 41:792–810

Grimmond CSB, Cleugh HA, Oke TR (1991) An objective urban heat storage model and its comparison with other schemes. Atmos Environ 25B:311–326

Grossman-Clarke S, Zehnder JA, Stefanov WL, Liu Y, Zoldak MA (2005) Urban modifications in a mesoscale meteorological model and the effects on near-surface variables in an arid metropolitan region. J Appl Meteorol 44:1281–1297

Grossman-Clarke S, Zehnder JA, Loridan T, Grimmond CSB (2010) Contribution of land use changes to near-surface air temperatures during recent summer extreme heat events in the Phoenix metropolitan area. J Appl Meteorol Climatol 49:1649–1664

Harlan S, Ruddell DM (2011) Climate change and health in cities: impacts of heat and air pollution and potential co-benefits from mitigation and adaptation. Curr Opin Environ Sustain 3:126–134

Harlan S, Brazel AJ, Prashad L, Stefanov WL, Larsen L (2006) Neighborhood microclimates and vulnerability to heat stress. Soc Sci Med 63:2847–2863

Harman IN, Belcher SE (2006) The surface energy balance and boundary layer over urban street canyons. Q J R Meteorol Soc 132:2749–2768

Hart MA, Sailor DJ (2009) Quantifying the influence of land-use and surface characteristics on spatial variability in the urban heat island. Theor Appl Climatol 95:397–406

Hawkins TW, Brazel AJ, Stefanov WL, Bigler W, Saffell EM (2004) The role of rural variability in urban heat island determination for Phoenix, Arizona. J Appl Meteorol 43: 476–486

House-Peters L, Chang H (2011) Modeling the impact of land use and climate change on neighborhood-scale evaporation and nighttime cooling: a surface energy balance approach, landscape and urban planning. Landsc Urban Plan 103:139–155

Imhoff ML, Zhang P, Wolfe RE, Bounoua L (2010) Remote sensing of the urban heat island effect across biomes in the continental USA. Remote Sens Environ 114:504–513

Järvi L, Grimmond CSB, Christen A (2011) The surface urban energy and water balance scheme (SUEWS). Evaluation in Los Angeles and Vancouver. J Hydrol 411: 219–237

JPL (Jet Propulsion Laboratory) (2001) ASTER higher-level product user guide. California Institute of Technology, Pasadena, CA

Karl TR, Melillo JM, Peterson TC (eds) (2009) Global climate change impacts in the United States. Cambridge University Press, New York, NY

Loridan T, Grimmond CSB, Offerle BD, Young DT, Smith T, Järvi L (2011) Local-scale urban meteorological parameterization scheme (LUMPS): longwave radiation parameterization and seasonality related developments.

J Appl Meteorol Climatol 50:185–202

Middel A, Brazel A, Hagen B, Myint SW (2011) Land cover modification scenarios and their effects on daytime heating in the inner core residential neighborhoods of Phoenix, AZ, USA. J Urban Technol 18:61–79

Middel A, Brazel AJ, Gober P, Myint SW, Chang H, Duh JD (in press) Land cover, climate, and the summer surface energy balance in Phoenix, AZ and Portland, OR. Int J Climatol

Myint SW, Okin GS (2009) Modelling land-cover types using multiple endmember spectral mixture analysis in a desert city. Int J Remote Sens 30:2237–2257

Myint SW, Gober P, Brazel A, Grossman-Clarke S, Weng Q (2011) Per-pixel vs. object-based classification of urban land cover extraction using high spatial resolution imagery. Remote Sens Environ 115:1145–1161

Nichol JE, Fung WY, Lam K, Wong MS (2009) Urban heat island diagnosis using ASTER satellite images and 'in situ' air temperature. Atmos Res 94:276–284

Offerle BD, Grimmond CSB, Oke TR (2003) Parameterization of net all-wave radiation for urban areas. J Appl Meteorol 42:1157–1173

Offerle B, Grimmond CSB, Fortuniak K, Pawlak W (2006) Intraurban differences of surface energy fluxes in a central European city. J Appl Meteorol Climatol 45:125–136

Palluconi FD, Hoover G, Alley R, Jentoft-Nilsen M (1994) Atmospheric correction method for ASTER thermal radiometry over land. Jet Propulsion Laboratory, California Institute of Technology, Pasadena, CA

Pearlmutter D, Krüger EL, Berliner P (2009) The role of evaporation in the energy balance of an open-air scaled urban surface. Int J Climatol 29:911–920

Ruddell DM, Harlan SL, Grossman-Clarke S, Buyantuyev A (2010) Risk and exposure to extreme heat in microclimates of Phoenix, AZ. In: Showalter PS, Lu Y (eds) Geospatial techniques in urban hazard and disaster analysis. Springer, New York, NY, p 179–202

Sarrat C, Lemonsu A, Masson V, Guedalia D (2006) Impact of urban heat island on regional atmospheric pollution. Atmos Environ 40:1743–1758

Shashua-Bar L, Pearlmutter D, Erell E (2009) The cooling efficiency of urban landscape strategies in a hot dry climate. Landsc Urban Plan 92:179–186

Shashua-Bar L, Pearlmutter D, Erell E (2011) The influence of trees and grass on outdoor thermal comfort in a hot-arid environment. Int J Climatol 31:1498–1506

Stewart ID, Oke TR (2010) Thermal differentiation of local climate zones using temperature observations from urban and rural field sites. In: Proc Ninth Symp Urban Environ, August 2010, Keystone, CO. AMS, p 1–7, http://ams.confex.com/ams/19Ag19BLT9Urban/webprogram/Paper173127.html

Stone B, Norman JM (2006) Land use planning and surface heat island formation: a parcel-based radiation flux approach. Atmos Environ 40:3561–3573

US Census Bureau (2010) 2010 census data. http://2010.census.gov/2010census/data/

Weng Q (2009) Thermal infrared remote sensing for urban climate and environmental studies: Methods, applications, and trends. ISPRS J Photogramm 64:335–344

Western Regional Climate Center (2011) Recent climate in the west. www.wrcc.dri.edu/

Xu W, Wooster MJ, Grimmond CS (2008) Modelling of urban sensible heat flux at multiple spatial scales: a demonstration using airborne hyperspectral imagery of Shanghai and a temperature–emissivity separation approach. Remote Sens Environ 112:3493–3510